Supporting Information for

Decoding episodes of past temperature spikes on the Martian surface using jarosite

Debdatta Banerjee, Swastika Chatterjee*

National Centre for High-Pressure Studies and Department of Earth Sciences,

Indian Institute of Science Education and Research-Kolkata, Mohanpur, Nadia - 741246, West Bengal, India.

*swastika@iiserkol.ac.in

Contents of this file

Texts S1-S9

Figures S1-S7

Tables S1-S5

Introduction

The overview of the supporting information is as follows:

- Site preference of Na in $K_{0.67}Na_{0.33}Fe_3(SO_4)_2(OH)_6$ (Jarosite-Natrojarosite solid-solution)
- The lattice parameters obtained after DFT (GGA) optimization of the crystal structures of Jarosites and the end products
- Total phonon density of states of Yavapaiite-Eldfellite solid solution;
- Relative thermodynamic stability of Jarosite and Natrojarosite with information regarding the decomposition of synthetic samples and coverage of temperature in the Martian context.
- Crystal structure of the monoclinic phase of Natrojarosite ($NaFe_3(SO_4)_2(OH)_6$)
- Comparison of the relative thermodynamic stability of Jarosite and Natrojarosite between the two different Natrojarosite phases (namely, monoclinic and trigonal)
- Total phonon density of states of K-jarosite and K-alunite solid solution
- Relative thermodynamic stability of K-Alunite and Na-Alunite
- The optimized lattice parameters for the case of Alunites

S1. Site preference of Na in $K_{0.67}Na_{0.33}Fe_3(SO_4)_2(OH)_6$ (jarosite-natrojarosite solid-solution)

A unit cell of jarosite contains 3 K-sites. Hence if 1 out of the 3-K is replaced by Na, we will attain a Na concentration of 33.33%. However, this single Na can occupy any one of the three available sites. To determine the site most preferred for Na occupancy, we have created three different configurations in each of which Na is doped at a different site. The total energy of all these configurations was determined using first principles density functional theory calculations. The configuration that had the lowest energy was adjudged the equilibrium structure and was used for rest of the analysis. Similar

calculations were done to determine the lowest energy configuration for 66.66% Na-doped jarosite. The lowest energy crystal structure for 33.33% Na doped jarosite is shown in Figure S1(a), whereas the relative energetics of the other configurations with 33.33% Na is shown in Figure S1(b).

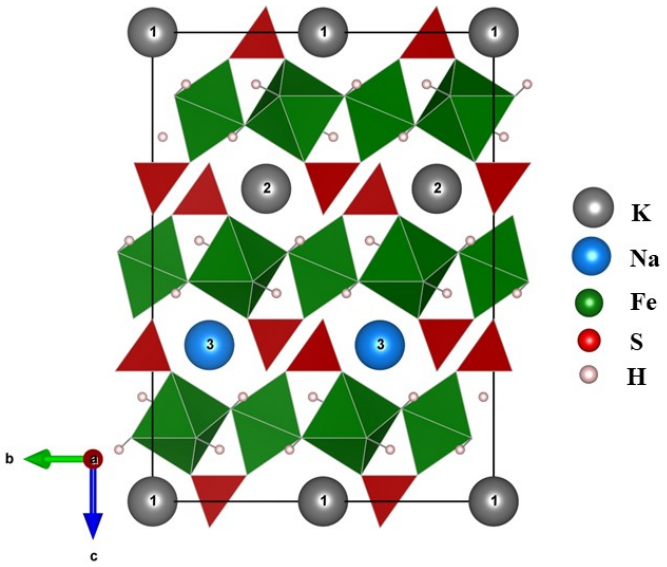

Figure S1(a). The lowest energy configuration of $K_{0.67}Na_{0.33}Fe_3(SO_4)_2(OH)_6$ (jarosite-natrojarosite solid-solution). The oxygen atoms are hidden in the figure for clarity.

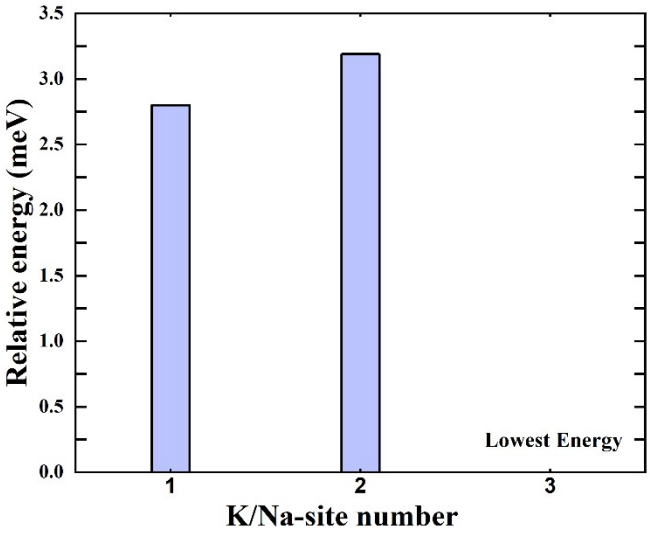

Figure S1(b). Relative energies of the 3 possible configurations of $K_{0.67}Na_{0.33}Fe_3(SO_4)_2(OH)_6$ (jarosite-natrojarosite solid-solution) scaled with respect to the lowest energy configuration. In the y-axis the numbers 1, 2, and 3 respectively denote the site-number (for *Na* occupancy) with reference to Figure S1(a). *Na* at site-3 hence corresponds to the lowest energy configuration (as shown in Figure S1(a)).

S2. The lattice parameters obtained after DFT (GGA) optimization of the crystal structures of jarosites and the end products

Table S1: The DFT (GGA) optimized crystal structure data of jarosite, natrojarosite, and jarosite-natrojarosite solid solution

Chemical Compositions	a(Å)	b(Å)	c(Å)	$\alpha(^\circ)$	$\beta(^\circ)$	$\gamma(^\circ)$	Method	References
JAROSITE - NATROJAROSITE								
$KFe_3SO_4(OH)_6$	7.391	7.391	17.568	90	90	120	DFT + U	This study
	7.291	7.291	17.174				XRD	Mills *et al.*, 2013
	7.302	7.302	17.204					Basciano & Petterson, 2007
	7.305	7.305	17.214					Whitworth, 2020
$(K_{0.67}Na_{0.33})\ Fe_3(SO_4)\ (OH)_6$	7.393	7.393	17.269	90	90	120	DFT + U	This study
$\sim(K_{0.6}Na_{0.4})\ Fe_3(SO_4)\ (OH)_6$	7.305	7.305	16.970				XRD	Basciano & Petterson, 2008
$(K_{0.33}Na_{0.67})\ Fe_3(SO_4)\ (OH)_6$	7.394	7.394	17.037	90	90	120	DFT + U	This study
$NaFe_3SO_4(OH)_6$ (Trigonal)	7.397	7.397	16.791	90	90	120	DFT + U	This study
	7.315	7.315	16.586				XRD	Basciano & Petterson, 2007
	7.318	7.318	16.623					Whitworth *et al.*, 2020
$NaFe_3SO_4(OH)_6$ (Monoclinic)	12.775	7.386	7.044	90	127.338	90	DFT + U	This study
	12.748	7.347	6.982		127.197		XRD	Scarlett *et al.*, 2010
	12.745	7.338	6.969		127.108		Neutron diffraction	Brand *et al.*, 2017

Table S2: The DFT (GGA) optimized crystal structure data of yavapaiite, eldfellite and hematite.

Chemical Compositions	a(Å)	b(Å)	c(Å)	$\alpha(^\circ)$	$\beta(^\circ)$	$\gamma(^\circ)$	Method	References
YAVAPAIITE - ELDFELLITE								
$KFe(SO_4)_2$	8.096	5.106	8.003	90	94.523	90	DFT + U	This study
	8.152	5.151	7.875		94.80		XRD	Forray *et al.*, 2005
	8.12	5.14	7.82		94.40			Hutton, 1959
	8.152	5.153	7.877		94.90			Graeber *et al.*, 1971
	7.90	5.07	7.84		93.78		DFT (HSE)	Chong *et al.*, 2017
$NaFe(SO_4)_2$	8.183	5.262	7.219		90.802		DFT + U	This study
	8.043	5.139	7.115		92.13		XRD	Balić-Žunić *et al.*, 2009
	7.90	5.07	7.31		90.86		DFT (HSE)	Chong *et al.*, 2017
HEMATITE								
Fe_2O_3	5.128	5.128	13.886	90	90	120	DFT + U	This study
	5.034	5.034	13.75				XRD	Finger and Hazen, 1980
	5.035	5.035	13.749					Fouad *et al.*, 2019
	5.040	5.040	13.763					Justus *et al.*, 2021
	5.059	5.059	13.801				DFT + U	Naveas *et al.*, 2023
	5.004	5.004	13.817				DFT + U + V (PBEsol)	

S3. Total phonon density of states of yavapaiite-eldfellite solid solution

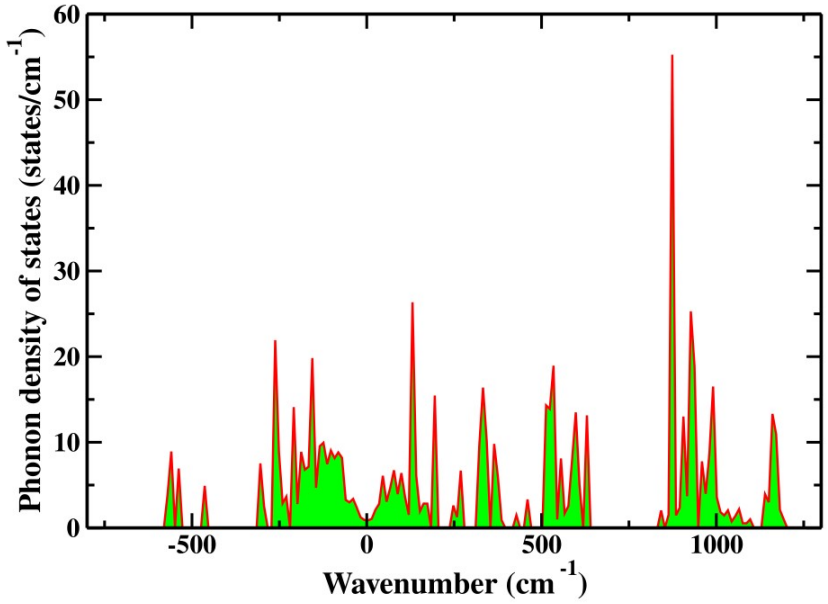

Figure S2. Total phonon density of states of yavapaiite-eldfellite solid solution $[K_{0.5}Na_{0.5}Fe_3(SO_4)_2(OH)_6]$

From the total phonon density of states (refer to Figure S2) for the solid solution of yavapaiite and eldfellite, significant imaginary frequencies can be observed. This indicates that this solid solution is dynamically unstable. Hence the possibility of considering this material as an end-product of jarosite-natrojarosite solid solution has been ruled out.

S4. Relative thermodynamic stability of Jarosite and Natrojarosite with information regarding the decomposition of synthetic samples and coverage of temperature in the Martian context

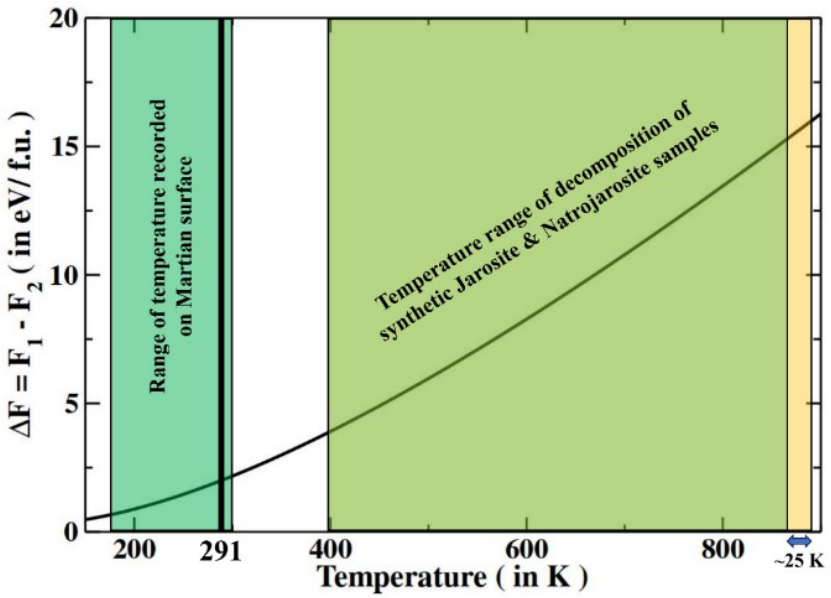

Figure S3. Relative thermodynamic stability of jarosite and natrojarosite highlighting relevant temperature conditions. Dark green: the complete temperature range prevailing on Martian surface; Light green: the temperature range along which jarosite-natrojarosite thermal breakdown takes place under terrestrial conditions. The bold line at 291K indicates the temperature at which the *K*-endmember jarosite is known to breakdown under Martian conditions [Navrotsky *et al.* 2005, Forray *et al.* 2005].

In the Figure S3, the relative thermodynamic stability of jarosite and natrojarosite has been shown. The complete temperature range recorded on the Martian surface has been indicated in dark green shade [Ohring and Marino (1968), Gómez-Elvira *et al.* (2012), Martírez *et al.* (2021), Rodriguez-Manfredi *et al.* (2021), Wordsworth *et al.* (2021), Atri *et al.* (2023)]. Note that very high temperatures (as included in the dark green shaded region) may be prevailing only at limited locations under special conditions. The 291 K line corresponds to the decomposition temperature of jarosite under Martian conditions [Navrotsky *et al.* 2005, Forray *et al.* 2005]. The relevant temperature range observed for the decomposition of synthetic jarosite and natrojarosite has been highlighted in light green. From previous studies it is observed that complete decomposition of natrojarosite occurs at a relatively lower temperature than jarosite, where the difference in temperature is ~25 K [Frost *et al.* 2005].

S5. Crystal structure of the monoclinic phase of Natrojarosite ($NaFe_3(SO_4)_2(OH)_6$)

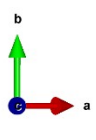

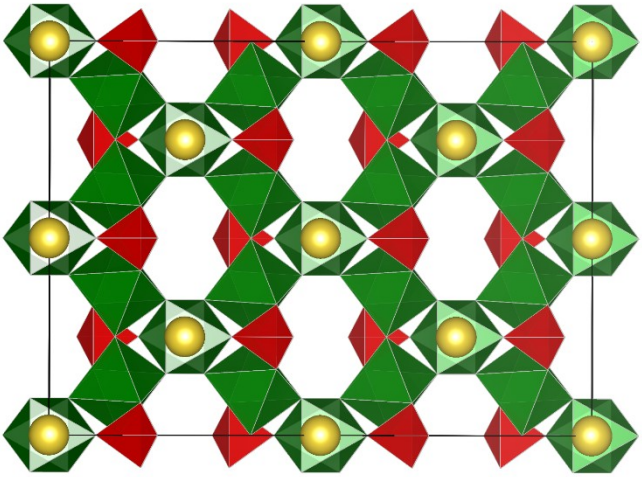

Figure S4. The crystal structure of natrojarosite in monoclinic symmetry. Here the golden atoms represent sodium (*Na*), green polyhedra contain iron (*Fe*) and the sulphur (*S*) sits in the red polyhedra.

S6. Comparison of the relative thermodynamic stability of jarosite and natrojarosite between the two different natrojarosite phases (namely, monoclinic and trigonal)

Natrojarosite ($NaFe_3(SO_4)_2(OH)_6$) is known to crystallize in two different polymorphs, namely the trigonal ($R\bar{3}m$) and monoclinic (C/2m). Our first-principles calculations suggest that the monoclinic natrojarosite is more stable than the trigonal form by 0.24 eV/f.u., at 0K, thereby indicating that the monoclinic natrojarosite is the low temperature polymorph as also suggested by experiments [Scarlett *et al.* (2010) & Brand et al. (2017)]. We have determined the relative thermodynamic stability of jarosite and the two different polymorphs of natrojarosite. Our thermodynamic calculations suggest that though the trigonal form of natrojarosite is less stable than jarosite, its low temperature monoclinic structure is more stable than *K*-end membered jarosite at all temperatures of interest as shown in Figure S5.

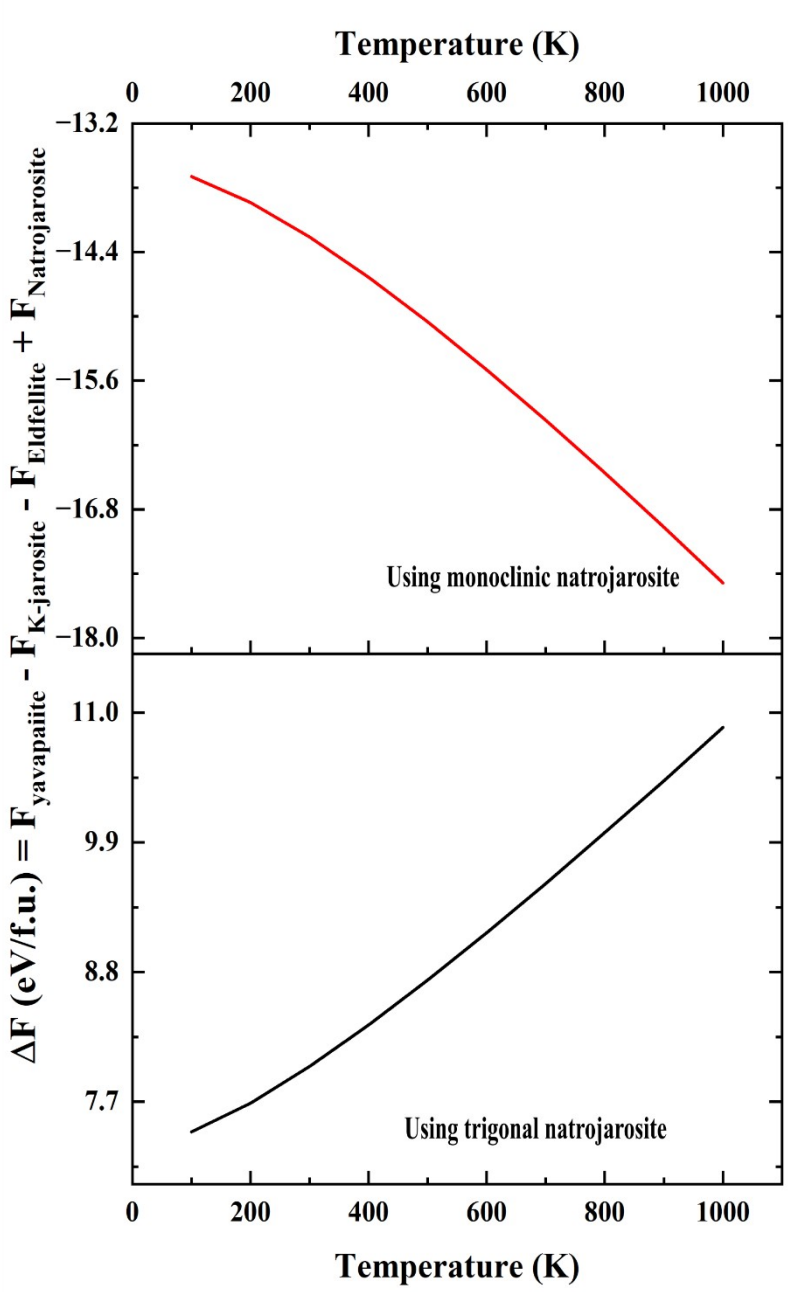

Figure S5. Relative thermodynamics stability of jarosite and natrojarosite: comparison for the two symmetries of natrojarosite

S7. Total phonon density of states of K-jarosite and K-alunite solid solution

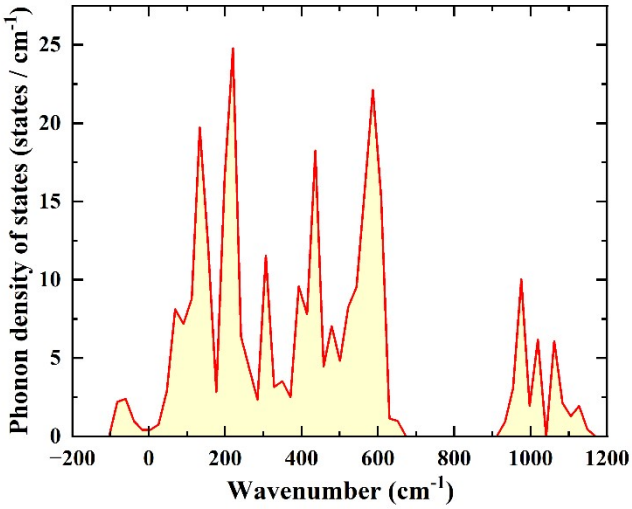

Figure S6. Total phonon density of states of K-jarosite and K-alunite solid solution $[K(Fe_{0.89}Al_{0.11})(SO_4)_2(OH)_6]$

From the total phonon density of states (Figure S6) for the solid solution of K-jarosite and K-alunite, significant imaginary frequencies can be observed. This indicates that this solid solution is dynamically unstable.

S8. (a) Relative thermodynamic stability of K-Alunite and Na-Alunite

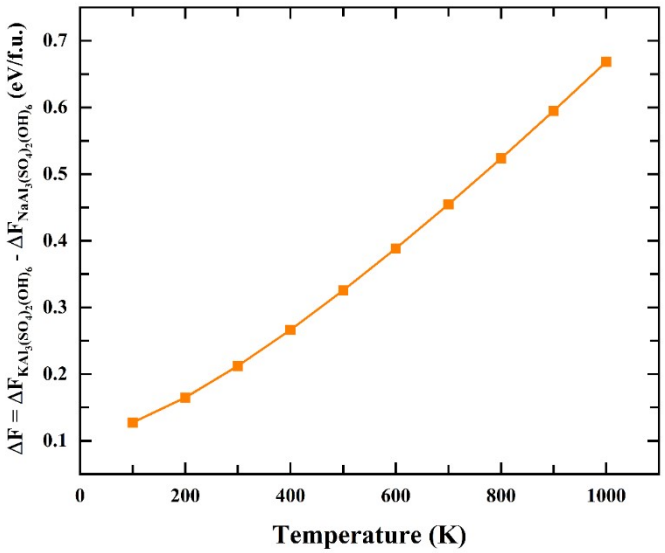

Figure S7(a). Relative change in Helmholtz energy with temperature for K-alunite and Na-alunite

$$KAl_3(SO_4)_2(OH)_6 \rightarrow KAl(SO_4)_2 + Al_2O_3 + 3H_2O \quad \text{----------} \ (S.a)$$

$$NaAl_3(SO_4)_2(OH)_6 \rightarrow NaAl(SO_4)_2 + Al_2O_3 + 3H_2O \quad \text{----------} \ (S.b)$$

$$\Delta F_a = F(KAl(SO_4)_2 + F(Al_2O_3) + 3F(H_2O) - F(KAl_3(SO_4)_2(OH)_6)$$

$$\Delta F_b = F(NaAl(SO_4)_2 + F(Al_2O_3) + 3F(H_2O) - F(NaAl_3(SO_4)_2(OH)_6)$$

$$\Delta F = \Delta F_a - \Delta F_b$$

Figure S7(a) graphically illustrates the relative change in Helmholtz energy ΔF (required for decomposition) for *K*-alunite & *Na*-alunite decomposition. We observe that $^{\Delta F} > 0$ which implies that *K*-alunite is thermodynamically more stable as compared to *Na*-alunite (or, natroalunite).

$XAl_3(SO_4)_2(OH)_6$ – Alunite, $XAl(SO_4)_2$ – Alum, Al_2O_3 – Aluminium oxide/Corundum

where, $X = K \text{ or } Na$

(b) Relative stability of Alunite-Jarosite mixtures and Jarosite:

Our study in conjugation with previous data suggests that since the solubility of Al^{3+} in jarosite is low, the solid solution will phase segregate into alunite and jarosite. An analysis of the relative thermodynamic stability of this mixture (of alunite (33%) and jarosite (67%)) with respect to 100% jarosite suggests that the mixture would be thermodynamically more stable. Our calculated results are presented below (Figure S7(b)). This energy does not fall in the coloured region of the plot in Figure 3 in the main manuscript.

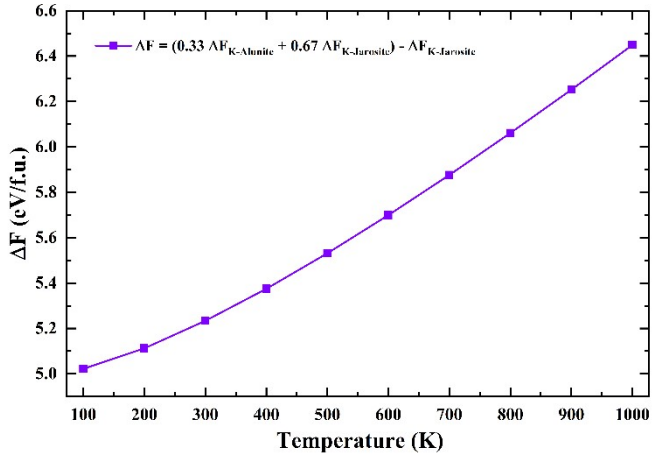

Figure S7(b). Difference in Helmholtz energy between the K-alunite-K-jarosite mineral assemblages (33% and 67% weightage, respectively) and K-jarosite, as a function of temperature.

S9. The optimized lattice parameters for the case of Alunites

Table S3. The DFT (GGA) optimized crystal structure data of K-alunite and natroalunite

Chemical Compositions	a(Å)	b(Å)	c(Å)	$\alpha(^\circ)$	$\beta(^\circ)$	$\gamma(^\circ)$	Method	References
ALUNITES								
$KAl_3(SO_4)_2(OH)_6$	7.063	7.063	17.637	90	90	120	DFT	This study
	7.000	7.000	17.180				XRD	Stoffregen & Alpers (1992) (150°C)
	6.975	6.975	17.315				XRD	Zema *et al.* (2012) (25°C)
$NaAl_3(SO_4)_2(OH)_6$	7.049	7.049	16.853				DFT	This study
	6.999	6.999	16.690				XRD	Stoffregen & Alpers (1992) (150°C)

Table S4. The DFT (GGA) optimized crystal structure data of corundum

Chemical Compositions	a(Å)	b(Å)	c(Å)	$\alpha(^\circ)$	$\beta(^\circ)$	$\gamma(^\circ)$	Method	References
CORUNDUM								
Al_2O_3	4.807	4.807	13.118	90	90	120	DFT	This study
	4.759	4.759	12.991				XRD	Newnham and Haan (1962)

Table S5. The DFT (GGA) optimized crystal structure data of K-alum and Na-alum

Chemical Compositions	a(Å)	b(Å)	c(Å)	$\alpha(^\circ)$	$\beta(^\circ)$	$\gamma(^\circ)$	Method	References
ALUMS								
	5.017	5.017	7.890	90	90	120	DFT	This study
	4.721	4.721	7.983				Neutron	West *et al.*

$KAl(SO_4)_2$							diffraction	(2008)
$NaAl(SO_4)_2$	7.993	5.075	7.179	90	90.874	90	DFT	This study

REFERENCES:

Atri, D., Abdelmoneim, N., Dhuri, D. B., & Simoni, M. (2023). Diurnal variation of the surface temperature of Mars with the Emirates Mars Mission: a comparison with Curiosity and Perseverance rover measurements. Monthly Notices of the Royal Astronomical Society: Letters, 518(1), L1-L6. [Crossref]

Balić-Žunic, T., Garavelli, A., Acquafredda, P., Leonardsen, E., & Jakobsson, S. P. (2009). Eldfellite, $NaFe(SO_4)_2$, a new fumarolic mineral from Eldfell volcano, Iceland. *Mineralogical Magazine*, 73(1), 51-57. [Crossref]

Basciano, L. C., & Peterson, R. C. (2007). Jarosite–hydronium jarosite solid-solution series with full iron site occupancy: mineralogy and crystal chemistry. *American Mineralogist*, 92(8-9), 1464-1473. [Crossref]

Basciano, L. C., & Peterson, R. C. (2008). Crystal chemistry of the natrojarosite-jarosite and natrojarosite-hydronium jarosite solid-solution series: A synthetic study with full Fe site occupancy. *American Mineralogist*, 93(5-6), 853-862. [Crossref]

Brand, H. E., Scarlett, N. V., & Knight, K. S. (2017). Thermal expansion of deuterated monoclinic natrojarosite; a combined neutron–synchrotron powder diffraction study. *Journal of Applied Crystallography*, 50(2), 340-348. [Crossref]

Chong, X. Y., Jiang, Y., & Feng, J. (2017). Mechanical properties, electronic structure and alkali-ion diffusion of Eldfellite-type $AFe(SO_4)_2$ (A= Li, Na, K) as potential cathode materials comparing with $LiFePO_4$. *Journal of Micromechanics and Molecular Physics*, 2(01), 1750002. [Crossref]

Finger, L. W., & Hazen, R. M. (1980). Crystal structure and isothermal compression of Fe_2O_3, Cr_2O_3, and V_2O_3 to 50 kbars. *Journal of Applied Physics*, 51(10), 5362-5367. [Crossref]

Forray, F. L., Drouet, C., & Navrotsky, A. (2005). Thermochemistry of yavapaiite $KFe(SO_4)_2$: Formation and decomposition. Geochimica et Cosmochimica Acta, 69(8), 2133-2140. [Crossref]

Fouad, D. E., Zhang, C., El-Didamony, H., Yingnan, L., Mekuria, T. D., & Shah, A. H. (2019). Improved size, morphology and crystallinity of hematite (α-Fe_2O_3) nanoparticles synthesized via the precipitation route using ferric sulfate precursor. *Results in Physics*, 12, 1253-1261. [Crossref]

Frost, R. L., Weier, M. L., & Martens, W. (2005). Thermal decomposition of jarosites of potassium, sodium and lead. Journal of thermal analysis and calorimetry, 82(1), 115-118. [Crossref]

Gómez-Elvira, J., et al., (2012). REMS: The environmental sensor suite for the Mars science laboratory rover. Space Science Reviews 170, 583-640. [Crossref]

Graeber, E. J., & Rosenzweig, A. (1971). The crystal structures of yavapaiite, $KFe(SO_4)_2$, and goldichite, $KFe(SO_4)_2 \cdot 4H_2O$. *American Mineralogist: Journal of Earth and Planetary Materials*, 56(11-12), 1917-1933. [Crossref]

HAAN, Y. D. (1962). Refinement of the a Al_2O_3, Ti_2O_3, V_2O_3 and Cr_2O_3 structures. Zeitschrift für Kristallographie-Crystalline Materials, 117(1-6), 235-237. [Crossref]

Hutton, C. O. (1959). Yavapaiite, an anhydrous potassium, ferric sulphate from Jerome, Arizona. *American Mineralogist: Journal of Earth and Planetary Materials*, 44(11-12), 1105-1114. [Crossref]

Justus, J. S., Roy, S. D. D., Saravanakumar, K., & Raj, A. M. E. (2021). Judging phase purity of hematite (α-Fe_2O_3) nanoparticles through structural and magnetic studies. *Materials Research Express*, 8(5), 055005. [Crossref]

Martínez, G. M., et al., (2021). The surface energy budget at gale crater during the first 2500 sols of the mars science laboratory mission. Journal of Geophysical Research: Planets, 126(9), e2020JE006804. [Crossref]

Mills, S. J., Nestola, F., Kahlenberg, V., Christy, A. G., Hejny, C., & Redhammer, G. J. (2013). Looking for jarosite on Mars: The low-temperature crystal structure of jarosite. *American Mineralogist*, 98(11-12), 1966-1971. [Crossref]

Navrotsky, A., Forray, F. L., & Drouet, C. (2005). Jarosite stability on Mars. Icarus, 176(1), 250-253. [Crossref]

Ohring G., Mariano J. (1968) Seasonal and latitudinal variations of the average surface temperature and vertical temperature profile on Mars. Journal of the atmospheric science 25 (8): 673. [Crossref]

Rodriguez-Manfredi, J. A., et al., (2021). The Mars Environmental Dynamics Analyzer, MEDA. A suite of environmental sensors for the Mars 2020 mission. Space Science Reviews 217(3):48. [Crossref]

Scarlett, N. V., Grey, I. E., & Brand, H. E. (2010). Ordering of iron vacancies in monoclinic jarosites. *American Mineralogist*, 95(10), 1590-1593. [Crossref]

Stoffregen, R. E., & Alpers, C. N. (1992). Observations on the unit-cell dimensions, H_2O contents, and δD values of natural and synthetic alunite. American Mineralogist, 77(9-10), 1092-1098. [Crossref]

West, D. V., Huang, Q., Zandbergen, H. W., McQueen, T. M., & Cava, R. J. (2008). Structural disorder, octahedral coordination and two-dimensional ferromagnetism in anhydrous alums. Journal of solid state chemistry, 181(10), 2768-2775. [Crossref]

Whitworth, A. J., Brand, H. E., & Frierdich, A. J. (2020). Iron isotope exchange and fractionation between jarosite and aqueous Fe (II). *Chemical Geology*, 554, 119802. [Crossref]

Wordsworth, R., Knoll, A. H., Hurowitz, J., Baum, M., Ehlmann, B. L., Head, J. W., & Steakley, K. (2021). A coupled model of episodic warming, oxidation and geochemical transitions on early Mars. Nature Geoscience, 14(3), 127-132. [Crossref]

Zema, M., Callegari, A. M., Tarantino, S. C., Gasparini, E., & Ghigna, P. (2012). Thermal expansion of alunite up to dehydroxylation and collapse of the crystal structure. Mineralogical Magazine, 76(3), 613-623. [Crossref]